An Ultracompact GRIN-Lens-Based Spot Size Converter using Subwavelength Grating Metamaterials

José Manuel Luque-González,* Robert Halir, Juan Gonzalo Wangüemert-Pérez, José de-Oliva-Rubio, Jens H. Schmid, Pavel Cheben, Íñigo Molina-Fernández, and Alejandro Ortega-Moñux

Graded-index materials offer virtually complete control over light propagation in integrated photonic chips but can be challenging to implement. Here, an anisotropic graded-index metamaterial, synthesized with fully etched silicon subwavelength structures, is proposed. Based on this material, a spot size converter that expands the transverse electric (TE) mode field profile from a 0.5 µm wide silicon wire waveguide to a 15 µm wide waveguide within a length of only 14 µm is designed. Measured insertion losses are below 1 dB in an unprecedented 130 nm bandwidth, limited by the measurement setup, with full 3D finite-difference time-domain (FDTD) simulations predicting a bandwidth in excess of 300 nm. Furthermore, the device is well suited to feed fiber-to-chip grating couplers, while requiring a footprint ten times smaller than conventional adiabatic tapers.

1. Introduction

Chip graded-index (GRIN) materials enable a plethora of different applications in optics such as light collimation,[1–3] waveguide crossings,[2] sharp multimode bends,[4,5] or invisibility cloaks.[6] Such materials can be implemented either through complex gray-scale lithography or by using subwavelength gratings (SWG). A subwavelength grating is a periodic dielectric structure with a period shorter than the wavelength propagating through it, thereby enabling the synthesis of metamaterials with a controllable equivalent refractive index using a single lithographic etch step.[7] Uniform (non-graded) SWGs have been used to demonstrate many high-performance devices in the silicon-on-insulator (SOI) platform,[7,8] including integrated biosensors,[9,10] ultrabroadband waveguide couplers,[11] and narrowband Bragg filters[12,13] among others. The anisotropy of such uniform SWGs

has recently been exploited to achieve advanced functionalities such as broadband behavior,[14] control of evanescent fields,[15] and high-performance polarization handling.[16–18] However, in graded-index metamaterials, the advantages of this intrinsic anisotropy remain unexplored.

In this work we demonstrate the use of an anisotropic SWG based GRIN material to implement an ultracompact, robust, and efficient spot size converter (**Figure 1**a). The GRIN profile is created by continuously changing the duty cycle (DC) of the SWG structure in the lateral direction (Figure 1b). We develop an anisotropic equivalent material model that shows that the anisotropy shortens the length of the device and enables a quick yet accurate way to design SWG based GRIN materials. Our lens achieves a spot-size conversion of the fundamental TE mode from a 0.5 µm wide silicon wire to a 15 µm wide waveguide in a total length of 14 µm, making it ten times shorter than a conventional taper. Compared to state-of-the-art spot-size converters[19–24] we achieve an unprecedented 130 nm bandwidth with measured insertion losses (IL) below 1 dB.

We furthermore show that the lens can be used to feed fiber-to-chip grating couplers from standard SOI waveguides with low losses. Indeed, the proposed GRIN lens SWG assisted spot size converter exhibits an exceptional combination of reduced footprint and insertion losses, as well as large bandwidth and tolerance to fabrication errors.

2. Implementing the Anisotropic GRIN Metamaterial

In a conventional isotropic GRIN lens, the refractive index profile follows a parabolic distribution.[25]

$$n_{\mathrm{GRIN}}(x) = n_{\max}\sqrt{1 - \alpha^2 x^2}, \quad \alpha = \frac{1}{\frac{w_{\mathrm{GRIN}}}{2}}\sqrt{1 - \left(\frac{n_{\min}}{n_{\max}}\right)^2} \quad (1)$$

where $n_{\max}$ and $n_{\min}$ are the refractive index at the center and the edges of the lens, w_{GRIN} is the width of the lens, and α is a parameter which measures the curvature of the refractive index parabola. From a ray optics point of view, an isotropic GRIN lens collimates

J. M. Luque-González, Dr. R. Halir, Prof. J. G. Wangüemert-Pérez, Dr. J. de-Oliva-Rubio, Prof. Í. Molina-Fernández, Dr. A. Ortega-Moñux
Departamento de Ingeniería de Comunicaciones, ETSI Telecomunicación
Universidad de Málaga
Campus de Teatinos s/n, 29010 Málaga, Spain
E-mail: jmlg@ic.uma.es
Dr. J. H. Schmid, Dr. P. Cheben
National Research Council Canada
1200 Montreal Road, Bldg. M50
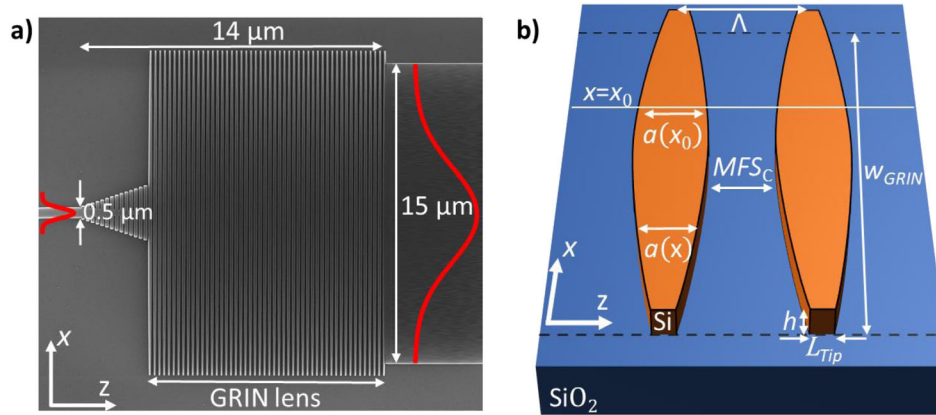Ottawa K1A 0R6, Canada

Figure 1. a) Scanning electron microscopy (SEM) image of the proposed spot size converter prior to the deposition of the SiO$_2$ cladding. The device converts the guided mode of a conventional 500 nm wide silicon wire to the fundamental mode of a 15 μm wide waveguide, with insertion losses below 1 dB. b) Schematic of the subwavelength structure. The shape of the silicon blocks $a(x)$ synthesizes the required index profile of the GRIN lens. The silicon dioxide cladding is not shown for clarity.

any paraxial input ray at a distance $f_{Ray} = \pi/2\alpha$.[25] Therefore, the design of a compact GRIN-lens-based spot size converter mainly relies on increasing the curvature of the parabola, α, to shorten the device length. However, the SWG structure exhibits an intrinsic anisotropy,[16] so that the equivalent refractive index along the z-direction differs significantly from the equivalent refractive index along the x-direction. As we will show later, this does not affect the device behavior, but significantly reduces its length when compared with the isotropic case. To take the anisotropy into account, we estimate the collimation distance via electromagnetic analysis of the modes of the structure, considering the GRIN lens as a multimode gradual index waveguide. Specifically, the collimation distance can be expressed as[26]

$$f_{EM} = L_{\frac{\pi}{2}} = \frac{\lambda_0}{4\left(n_{eff0} - n_{eff1}\right)} \quad (2)$$

where n_{eff0} and n_{eff1} are the effective indices of the fundamental and first order modes, respectively. It can be shown that the collimation distance is wavelength independent for a non-dispersive parabolic GRIN material.[26]

The design parameters of an SWG based GRIN lens are (see Figure 1b): i) the width of the multimode region, w_{GRIN}, which enables us to reach the desired output beam width, ii) the shape of the silicon blocks, $a(x) = DC(x)\Lambda$, which implements the required parabolic refractive index profile of the GRIN lens, and iii) the period of the structure, Λ, which optimizes the bandwidth behavior, as we will show later. First, we set $w_{GRIN} = 16$ μm, only slightly wider than the desired output width to keep the curvature α as high as possible. For periods large enough to be readily fabricated, the device does not operate in the deep subwavelength regime, so that the shape $a(x)$ which synthesizes the required refractive index profile depends on the period, Λ. Hence, both parameters have to be designed simultaneously. We consider periods in the range of $\Lambda = 180$ nm to $\Lambda = 180$ nm to fulfil fabrication constraints and avoid Bragg reflections, respectively.

We now discuss the design process of the shape $a(x)$ for an intermediate period ($\Lambda = 240$ nm) and illustrate our anisotropic GRIN homogenization approach. We assume that the local equiv-

alent refractive index at any position x_0 along the GRIN lens (Figure 1b), is given by the equivalent refractive index of an x-invariant SWG waveguide with the same duty cycle and period (**Figure 2**: Inset). The core of this SWG structure can be approximated by a homogeneous anisotropic uniaxial material with permittivity tensor $\varepsilon(DC) = \text{diag}[n_{xx}^2(DC), n_{yy}^2(DC), n_{zz}^2(DC)]$[16] which, for a given period, depends only on the duty cycle. Therefore, we can calculate a look-up table which maps a desired refractive index into its corresponding duty cycle as follows. First, we obtain $n_{xx}(DC)$ by computing the effective index of the fundamental x-polarized Floquet–Bloch mode propagating along the z-direction in the structure shown in the inset of Figure 2 (the blue arrow indicates the propagation direction). The equivalent index n_{xx} is then given by the refractive index of a homogeneous isotropic slab waveguide whose fundamental TE mode has the same effective index as the Floquet–Bloch mode. Then, we obtain $n_{zz}(DC)$, by proceeding analogously with the z-polarized Floquet mode propagating along the x-axis (Figure 2: Inset, red arrow). For illustration purposes in this figure we assume a 220-nm-thick SOI platform at $\lambda_o = 1.55$ μm and, referring to Figure 1b, a typical tip width $L_{Tip} = 50$ nm on the edge of the lens, and a MFS_C of 80 nm in the center. Note that in the Supporting Information we demonstrate the proposed methodology for other silicon thicknesses. These values yield a duty cycle range from $DC_{min} = L_{Tip}/\Lambda \approx 0.2$ to $DC_{max} = 1 - MFS_C/\Lambda \approx 0.65$, obtaining the look-up table relations shown in Figure 2. We then impose that $n_{xx}(x)$ follow the parabolic law in Equation (1) and use the look-up table to obtain both the shape of the silicon blocks, $a(x) = DC(x)\Lambda$, as well as the value of n_{zz} implemented by this duty cycle.

To validate our model, we compare 3D-FDTD simulations of the periodic lens structure (**Figure 3**a) with a homogenous anisotropic lens (Figure 3b) and a homogenous isotropic lens (Figure 3c), when they are illuminated by 3×0.22 μm^2 (width by height) Gaussian beam. In the periodic lens structure the periods are shaped as determined by the algorithm presented in Figure 2. In Figure 3 we have indicated with a black dashed line the distance where the beams have been fully expanded and collimated. Three important conclusions can be drawn from Figure 3: i) the proposed structure works as a spot size converter (Figure 3a),
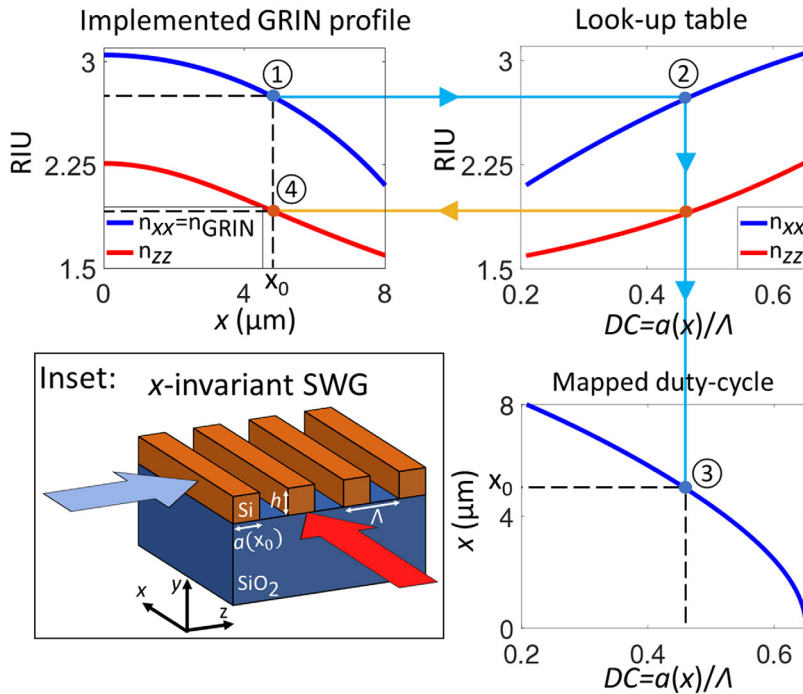
Figure 2. To implement the equivalent refractive index $n_{xx}(x_0) = n_{GRIN}(x_0)$ at any position x_0, (marked as ①) we refer to a look-up table (marked as ②) constructed by analyzing the structure shown in the inset, obtaining the shape $a(x_0)$ (marked as ③). This in turn imposes the value of $n_{zz}(x_0)$ (marked as ④). Inset: Schematic of the periodic structure used to calculate both polarizations of the look-up table. Typical SOI values, $n_{Si} = 3.476$, $n_{SiO_2} = 1.444$, $h = 0.22$ μm, and a period $\Lambda = 0.24$ μm are assumed.

ii) it can be accurately homogenized as an anisotropic graded-index metamaterial (compare Figure 3a,b), and iii) the isotropic homogenization does not emulate the z-periodic structure behavior (compare Figure 3a,c). Note that the formula $f_{Ray} = \pi/(2\alpha)$, with α as defined in Equation (1), predicts a 17 μm collimation distance for the isotropic approach, close to the simulated isotropic value. Otherwise, by computing the effective indexes of the two lowest order modes of the gradual anisotropic waveguide (Figure 3b) and applying Equation (2), a 12 μm collimation distance is obtained, very close to the 11 μm of the periodic structure. Therefore, the anisotropic model can be used to design the proposed GRIN lens with an anisotropic mode solver which is much faster than 3D-FDTD simulations. A similar analysis to the one performed in Figure 3 has been carried out for the transverse magnetic (TM) mode in the Supporting Information, showing that the metamaterial still works as a spot size converter, but requires a longer device, since TM polarization does not benefit from the anisotropy mediated shortening of the collimation distance.[16]

3. Numerical Optimization of the GRIN Lens Spot Size Converter

We now design the shape of the silicon blocks $a(x)$ using the anisotropic model outlined in the previous section to seek a short, robust, and broadband GRIN lens. **Figure 4**a shows the

collimation distance as a function of the minimum feature size in the center of the lens $MFS_C = (1 - DC_{max})\Lambda$ for different periods in the range $\Lambda = 180$ nm to $\Lambda = 260$ nm. In these simulations, we fixed the lens width $w_{GRIN} = 16$ μm and the tip width $L_{Tip} = DC_{min}\Lambda = 50$ nm (Figure 1b), that is, we maintained n_{min} while changing n_{max}. Note that each value of MFS_C implies a different refractive index profile $n_{GRIN}(x)$, and therefore also a different shape of the silicon blocks $a(x)$ (Figure 4a: Inset). This calculation has been carried out by using the proposed anisotropic GRIN model to calculate the modes of the multimode gradual index anisotropic waveguide and then applying Equation (2) to estimate the collimation distance. Figure 4a reveals that the minimum collimation distance, marked with a dot for each period, is not achieved when the ratio n_{max}/n_{min} is maximum ($DC_{max} = 1 \Rightarrow MFS_C = 0$) as would be the case in an isotropic GRIN lens (see Equation (1)). This behavior is auspicious because it implies that the optimum MFS_C for a shorter device depends on the period and it is in the range of 50–90 nm. A flatter curve around the design point in Figure 4a indicates that the device will be more tolerant to fabrication errors. We then calculate the wavelength dependence of the collimation distance assuming its optimum MFS_C for each period (Figure 4b). Although longer periods imply a shorter collimation distance, the equivalent metamaterial becomes more dispersive at shorter wavelengths, because of the proximity to the Bragg regime. The metamaterial dispersion changes the collimation distance as shown in Figure 4b, thereby detuning the device and increasing the insertion losses at short wavelengths. Therefore, from Figure 4a,b we conclude that the period should be set to 240 nm with a minimum feature size $MFS_C \approx 80$ nm in the center, achieving a flat dispersion behavior with a fabricable MFS. Finally, we refine the length of the GRIN lens via 3D-FDTD simulations, obtaining a final lens length of 10.5 μm, just 1 μm shorter than the anisotropic estimation. If we excite the designed z-periodic GRIN lens directly from the 0.5 μm width photonic wire waveguide (butt-coupling), the insertion loss of the device is about 2 dB at the central wavelength. To improve the lens performance, we have designed a short (15 periods long) input taper, as it is shown in Figure 1a. The role of this taper is twofold: i) To provide a smooth transition between the input silicon wire and the z-periodic structure, and ii) to ensure that the higher order modes of the lens are not excited. Note that the beam collimation condition of a GRIN lens requires the paraxial approximation,[25] which is not satisfied for such higher order modes. To design the input taper we apply a two-step procedure: First, we determine, by using 3D-FDTD simulations, the minimum length of the taper to assure negligible transition losses and back-reflections between the photonic wire at the input and the GRIN metamaterial. In this step, we keep the output taper width constant. Second, we optimize the output width of the taper to minimize the insertion loss of the whole
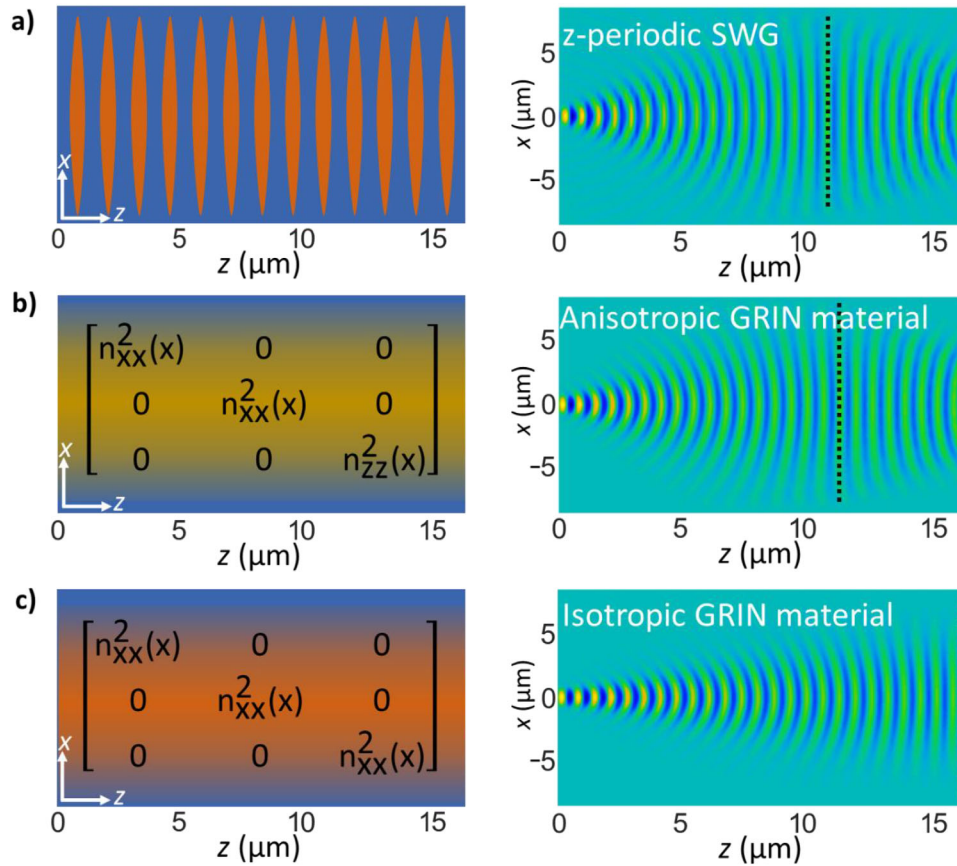
Figure 3. Schematic of the structure (left) and real part of the 3D-FDTD simulated main component of the TE polarized electric field propagation, $\mathcal{R}e\{E_x(x,z)\}$, along the proposed GRIN lens (right) implemented with: a) a z-periodic SWG structure, b) a gradual anisotropic material, and c) a gradual isotropic material.

device. With this two-step approach, we achieve a reduction of the simulated insertion loss from 2 dB (butt-coupling) to 0.5 dB (with optimized adaptation taper). Final device dimensions are summarized in **Table 1**. In **Figure 5**a we show the simulated IL of the resulting spot size converter, achieving IL <1 dB in a bandwidth exceeding 300 nm.

4. Fabrication and Characterization

In order to experimentally demonstrate the proposed structure, a set of SWG GRIN lens spot size converters have been fabricated in a 220 nm thick SOI platform. The buried oxide (BOX) and the upper SiO_2 cladding are 2 µm and 2.2 µm thick, respectively.[27] The spot size converter has been fabricated with the nominal parameters (Table 1) and ±10% duty cycle offsets to study the tolerances of the device. We included a set of back-to-back lenses cascaded multiple times to obtain the insertion loss of one GRIN lens (cutback configuration).

Light from a tunable laser (Agilent 81600B) connected to a lensed polarization maintaining fiber (PMF) is coupled into the chip using an SWG edge coupler.[28–30] The PMF is mounted on a rotatory stage, which, together with a Glan–Thompson polarizer at the output allows us to control the polarization on the chip. At the chip output, light is focused onto a photodetector

(818-IR) using a microscope objective. The transmission spectrum is measured by sweeping the wavelength of the tunable laser while recording the output power. Figure 5b shows the normalized measured output power at the central wavelength of the measured band ($\lambda = 1.58$ µm) as a function of the number of cascaded lenses. Insertion losses below 1 dB of are achieved even with a ±10% offset in the duty cycle, indicating a good tolerance to fabrication deviations. As a reference, a conventional linear taper with a length of 150 µm exhibits comparable insertion losses of ≈1 dB. Figure 5a draws the simulated (dashed blue line) and measured (solid blue line) insertion losses of the nominal SWG GRIN lens spot size converter. Spurious reflections have been removed using the minimum phase technique.[31] These measurements confirm that our device shows an excellent performance in terms of insertion losses, with IL < 0.6 dB at the central wavelength, maintaining the IL < 1 dB in a bandwidth from 1.51 to 1.64 µm limited by our setup, extending beyond 1.8 µm according to our simulations. In **Table 2** we summarize the main characteristic of state-of-the-art spot-size-converters (SSC) in the SOI platform. To compare different expansion ratios, (ER = w_{out}/w_{in}), we use the normalized expansion ratio (NER).[23]

$$\text{NER}(\lambda) = \frac{w_{out}/w_{in}}{L/\lambda} \cdot IL(\lambda) = \overline{ER} \cdot IL(\lambda) \tag{3}$$

**ADVANCED
SCIENCE NEWS**

www.advancedsciencenews.com

**LASER
& PHOTONICS
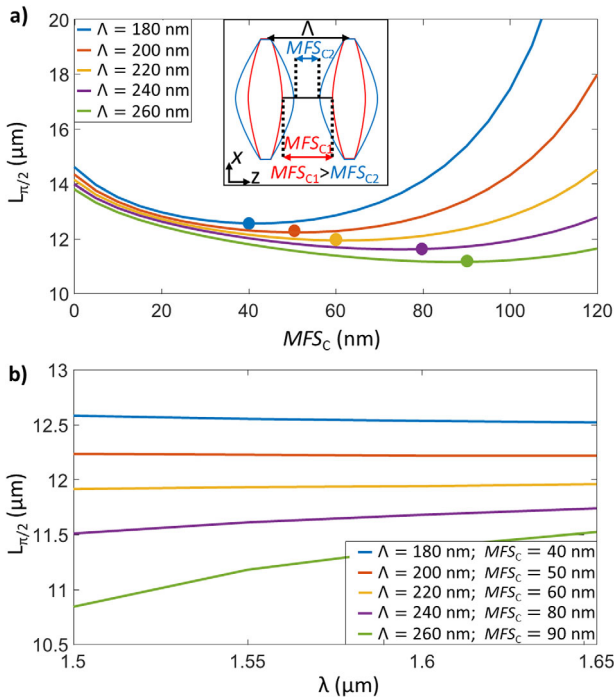REVIEWS**

www.lpr-journal.org

Figure 4. a) Collimation distance as a function of the gap in the center of the lens (MFS_C) calculated for different periods as obtained through modal analysis of the homogenized anisotropic structure. Inset: Schematic of the period shape variation when changing the MFS_C maintaining w_{GRIN} and L_{Tip}. b) Collimation distance dispersion assuming the optimum MFS_C for each period (marked with solid circles in Figure 4a).
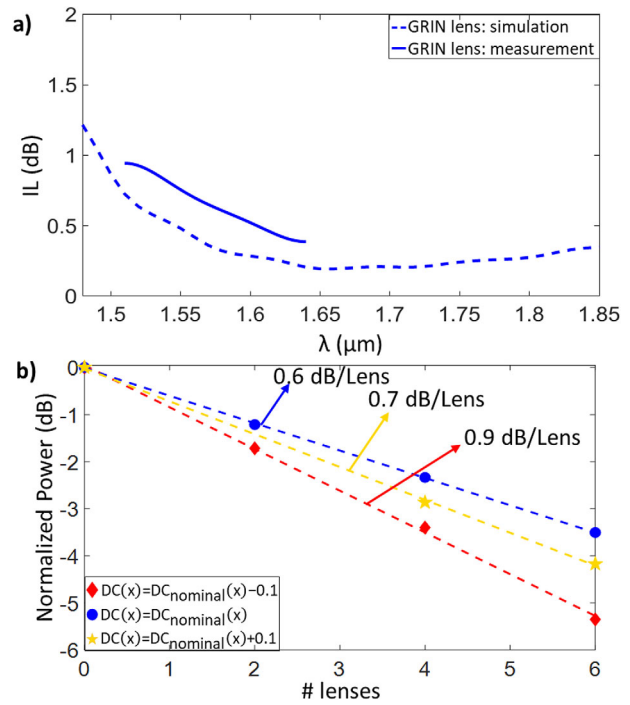

Figure 5. a) Insertion losses as a function of the wavelength for the nominal SWG lens design (blue lines). Measurements were performed using a back-to-back configuration, so measured insertion losses are divided by two. Our measurement setup is limited to the 1.51 μm < λ < 1.64 μm wavelength range. b) Measured transmitted power as a function of the number of GRIN lenses at λ = 1.58 μm Three different structures have been characterized: the nominal design and two lenses with duty cycle offsets of ±10%, respectively.

Table 1. Geometrical parameters of the proposed spot-size converter.

GRIN lens		
	w_{GRIN} = 16 μm	Λ = 240 nm
	L_{Tip} = 50 nm	$a(x)$: see Figure 2
	MFS_C = 80 nm	44 periods
Input taper	Λ = 240 nm	DC = 0.65
	$w_{InTaper}$ = 0.5 μm	$w_{OutTaper}$ = 2.5 μm
	15 periods	

Table 2. Performance of some state-of-the-art spot size converters.

Structure	IL [dB]	BW [nm]	w_{out} [μm]	ER	L [μm]	NER [λ_0]	Ref.
Seg. taper	<1[a]	N/A	2[a]	4[a]	1.5[a]	3.7[a]	[19]
Lens assisted taper	<1	80	10	22	21	1.32	[20]
Seg. taper	<1	50	12	24	20	1.86	[21]
Adiabatic taper	<1	N/A	12	24	150	0.24	[22]
Semi lens	<1	50	10	20	10	2.85	[23]
Hollow taper	1.4[a]	43[a]	15[a]	50[a]	60[a]	0.9[a]	[24]
This work	<1	130	15	30	15	2.90	–

[a] Simulation results.

where w_{out} and w_{in} are the widths of the output and input waveguides, L is the length of the spot size converter, λ is the wavelength of the propagating light, and IL are the insertion losses (in linear scale). The first term of Equation (3), ($\overline{ER}$), defines the expansion ratio normalized to the electrical length of the beam expander. As a reference, for a Gaussian beam propagating through a homogeneous anisotropic material, this term can be calculated as $\overline{ER} = \frac{4 \cdot \lambda^2 \cdot n_{xx}}{\pi \cdot w_{in}^2 \cdot n_{zz}^2}$. This expression can be considered as an upper limit for the NER of a beam expander (see Supporting Information). Our lens provides an excellent NER over an extremely broad bandwidth compared to the state-of-the-art.

As a further validation, we have used our spot size converter to feed a pair of grating couplers in a back-to-back configuration (**Figure 6**a,b: Inset). Note that opposed to beam expansion in a free space slab, which results in a curved phase-front and

thus requires specialized focusing grating couplers,[32] our spot sizes converter creates a flat phase-front and can therefore directly replace an adiabatic taper. In this case, the measurement setup changes slightly: light from the laser is now coupled into a conventional SMF-28 fiber and the polarization is set to the desired TE state using a polarization controller (Agilent 8169A). Figure 6b compares the measured power when gratings are fed with a 150 μm linear taper and with our spot size converters. In terms of insertion losses the designed GRIN lens shows a behavior similar to a linear 150 μm long taper, even when coupling to a grating coupler that is specifically designed for the latter. For the nominal GRIN lens, we observed comparatively high
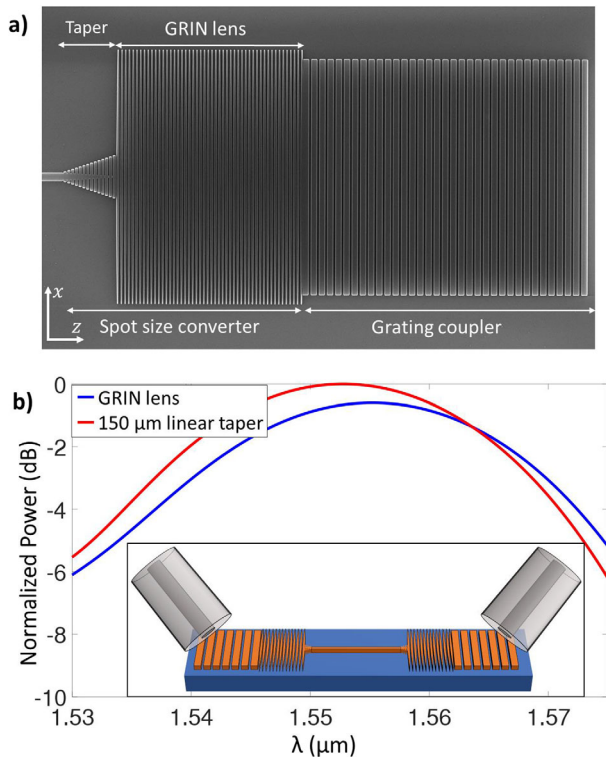
Figure 6. a) SEM image of the transition from a conventional 0.5 µm wide silicon wire waveguide to a 15 µm wide grating coupler, through the SWG GRIN lens spot size converter. b) Measured wavelength response of a surface grating coupler fed with: a conventional 150 µm length linear taper (red line) and the SWG GRIN lens expander (blue line). The curves have been normalized to the maximum coupling efficiency of the red curve to facilitate the comparison. Inset: Schematic of the back-to-back grating coupler configuration, fed with a pair of the SWG GRIN lens spot size converters.

back-reflections of 14% due to the index mismatch between the lens and the grating. The back-reflections can be reduced by adding a properly designed transition between the GRIN lens and the grating coupler.[33] In this case, the +15% duty cycle offset GRIN lens yields a reduction of back-reflections to 8%, without significant impact on insertion losses.

5. Conclusion

We have reported a compact spot size converter based on an anisotropic GRIN lens based on an SWG metamaterial structure. The proposed device expands a TE field profile 30 times over a distance of only 14 µm, with insertion loss under 1 dB in a measured bandwidth of 130 nm, while simulation predicts a bandwidth in excess of 300 nm. Compared with state-of-the-art devices, our lens achieves an excellent expansion ratio with outstanding bandwidth and is robust to fabrication errors. The device has been utilized to feed a grating coupler with compelling results. Our anisotropic homogenization strategy enables fast yet accurate simulations of the GRIN metamaterial and we believe that it opens up promising new routes for on-chip light handling.

[1] U. Levy, M. Abashin, K. Ikeda, A. Krishnamoorthy, J. Cunningham, Y. Fainman, *Phys. Rev. Lett.* **2007**, *98*, 243901.
[2] Q. Wu, J. P. Turpin, D. H. Werner, *Light: Sci. Appl.* **2012**, *1*, e38.
[3] P. Lalanne, P. Chavel, *Laser Photonics Rev.* **2017**, *11*, 1600295.
[4] L. H. Gabrielli, D. Liu, S. G. Johnson, M. Lipson, *Nat. Commun.* **2012**, *3*, 1216.
[5] H. Xu, Y. Shi, *Laser Photonics Rev.* **2018**, *12*, 1700240.
[6] J. Li, J. B. Pendry, *Phys. Rev. Lett.* **2008**, *101*, 203901.
[7] P. Cheben, R. Halir, J. H. Schmid, H. A. Atwater, D. R. Smith, *Nature* **2018**, *560*, 565.
[8] R. Halir, A. Ortega-Moñux, D. Benedikovic, G. Z. Mashanovich, J. G. Wangüemert-Pérez, J. H. Schmid, Í. Molina-Fernández, P. Cheben, *Proc. IEEE* **2018**, *106*, 2144.
[9] J. Gonzalo Wangüemert-Pérez, P. Cheben, A. Ortega-Moñux, C. Alonso-Ramos, D. Pérez-Galacho, R. Halir, Í. Molina-Fernández, D. Xu, J. H. Schmid, *Opt. Lett.* **2014**, *39*, 4442.
[10] L. Torrijos-Morán, J. García-Rupérez, *Opt. Express* **2019**, *27*, 8168.
[11] H. Yun, L. Chrostowski, N. A. F. Jaeger, *Opt. Lett.* **2018**, *43*, 1935.
[12] J. Čtyroký, J. G. Wangüemert-Pérez, P. Kwiecien, J. Litvik, J. H. Schmid, Í. Molina-Fernández, A. Ortega-Moñux, M. Dado, P. Cheben, *Opt. Express* **2018**, *26*, 3041.
[13] P. Cheben, J. Čtyroký, J. H. Schmid, S. Wang, J. Lapointe, J. G. Wangüemert-Pérez, Í. Molina-Fernández, A. Ortega-Moñux, R. Halir, D. Melati, D. Xu, S. Janz, M. Dado, *Opt. Lett.* **2019**, *44*, 1043.
[14] R. Halir, P. Cheben, J. M. Luque-González, J. D. Sarmiento-Merenguel, J. H. Schmid, G. Wangüemert-Pérez, D.-X. Xu, S. Wang, A. Ortega-Moñux, Í. Molina-Fernández, *Laser Photonics Rev.* **2016**, *10*, 1039.
[15] S. Jahani, S. Kim, J. Atkinson, J. C. Wirth, F. Kalhor, A. Al Noman, W. D. Newman, P. Shekhar, K. Han, V. Van, R. G. DeCorby, L. Chrostowski, M. Qi, Z. Jacob, *Nat. Commun.* **2018**, *9*, 1893.
[16] J. M. Luque-González, A. Herrero-Bermello, A. Ortega-Moñux, Í. Molina-Fernández, A. V. Velasco, P. Cheben, J. H. Schmid, S. Wang, R. Halir, *Opt. Lett.* **2018**, *43*, 4691.
[17] H. Xu, D. Dai, Y. Shi, *Laser Photonics Rev.* **2019**, *1800349*, 1.

**ADVANCED
SCIENCE NEWS**

www.advancedsciencenews.com

LASER
& PHOTONICS
REVIEWS

www.lpr-journal.org

[18] A. Herrero Bermello, J. M. Luque-González, A. Velasco, A. Ortega-Moñux, P. Cheben, R. Halir, *IEEE Photonics J.* **2019**, *11*, 6601508.

[19] B. Luyssaert, P. Bienstman, P. Vandersteegen, P. Dumon, R. Baets, *J. Lightwave Technol.* **2005**, *23*, 2462.

[20] K. Van Acoleyen, R. Baets, in *8th IEEE Int. Conf. on Group IV Photonics*, IEEE, Piscataway, NJ, USA **2011**, pp. 157–159.

[21] J. Zou, Y. Yu, M. Ye, L. Liu, S. Deng, X. Xu, X. Zhang, *Opt. Lett.* **2014**, *39*, 6273.

[22] Y. Fu, T. Ye, W. Tang, T. Chu, *Photonics Res.* **2014**, *2*, A41.

[23] S. Abbaslou, R. Gatdula, M. Lu, A. Stein, W. Jiang, *Opt. Lett.* **2017**, *42*, 4383.

[24] M. Asaduzzaman, M. Bakaul, E. Skafidas, M. R. H. Khandokar, *Sci. Rep.* **2018**, *8*, 2540.

[25] B. E. A. Saleh, M. C. Teich, *Fundamentals of Photonics*, John Wiley & Sons, New York **1991**.

[26] S. El-Sabban, D. Khalil, *Opt. Eng.* **2015**, *54*, 037103.

[27] NanoSOI Fabrication process. Applied Nanotools Inc. https://www.appliednt.com/nanosoi/ (accessed: September 2019).

[28] P. Cheben, D.-X. Xu, S. Janz, A. Densmore, *Opt. Express* **2006**, *14*, 4695.

[29] P. Cheben, P. J. Bock, J. H. Schmid, J. Lapointe, S. Janz, D.-X. Xu, A. Densmore, A. Delâge, B. Lamontagne, T. J. Hall, *Opt. Lett.* **2010**, *35*, 2526.

[30] P. Cheben, J. H. Schmid, S. Wang, D. Xu, M. Vachon, S. Janz, J. Lapointe, Y. Painchaud, M. Picard, *Opt. Express* **2015**, *23*, 22553.

[31] R. Halir, Í. Molina-Fernández, J. G. Wangüemert-Pérez, A. Ortega-Moñux, J. De-Oliva-Rubio, P. Cheben, *Opt. Express* **2009**, *17*, 8349.

[32] F. Van Laere, S. Member, T. Claes, J. Schrauwen, S. Scheerlinck, W. Bogaerts, D. Taillaert, *IEEE Photonics Technol. Lett.* **2007**, *19*, 1919.

[33] D. Benedikovic, C. Alonso-Ramos, D. Pérez-Galacho, S. Guerber, V. Vakarin, G. Marcaud, X. Le Roux, E. Cassan, D. Marris-Morini, P. Cheben, F. Boeuf, C. Baudot, L. Vivien, *Opt. Lett.* **2017**, *42*, 3439.